Free-surface and internal multiple elimination in one step without adaptive subtraction

Zhang, Lele; Slob, Evert

DOI
10.1190/geo2018-0548.1

Publication date
2019

Document Version
Final published version

Published in
Geophysics

GEOPHYSICS, VOL. 84, NO. 1 (JANUARY-FEBRUARY 2019); P. A7–A11, 4 FIGS.
10.1190/GEO2018-0548.1

Free-surface and internal multiple elimination in one step without adaptive subtraction

Lele Zhang[1] and Evert Slob[2]

ABSTRACT

We have derived a scheme for retrieving the primary reflections from the acoustic surface-reflection response by eliminating the free-surface and internal multiple reflections in one step. This scheme does not require model information and adaptive subtraction. It consists only of the reflection response as a correlation and convolution operator that acts on an intermediate wavefield from which we compute and capture the primary reflections. For each time instant, we keep one value for each source-receiver pair and store it in the new data set. The resulting data set contains only primary reflections, and from this data set, a better velocity model can be built than from the original data set. A conventional migration scheme can then be used to compute an artifact-free image of the medium. We evaluated the success of the method with a 2D numerical example. The method can have a wide range of applications in 3D strongly scattering media that are accessible from one side only.

INTRODUCTION

The processing of reflection of acoustic or elastodynamic waves plays a central role in seismic exploration and seismology. Multiple reflection is a common phenomenon that occurs in media in which the velocity or density varies with position. For seismology and seismic exploration, the measured data contain multiple reflections caused by the heterogeneity of the earth. The measured data are the reflection response of the subsurface generated by the signal emitted by an active source acting on the surface and observed by receivers located up to kilometers away from the source. The measured data appear as a first arrival followed by coda waves. The multiple reflections present in the measured data degrade the quality of the image (Weglein, 2016) because imaging schemes assume that only primary reflections have occurred in the medium. Our aim is to find a way to remove free-surface and internal multiple reflections from the measured data set in one step without model information and adaptive filtering.

Several schemes have been developed to mitigate the artifacts in the image that are caused by multiple reflections. Some of them focus on removing free-surface or internal multiple reflections from the measured single-sided reflection response in the data domain, such as surface-related multiple elimination (SRME) (Verschuur et al., 1992) and the inverse scattering series (ISS) (Weglein et al., 1997). For SRME, the free-surface-related multiple reflections can be removed with a minimum-energy criterion. For ISS, internal multiple reflections can be predicted approximately (Ten Kroode, 2002; Löer et al., 2016). Van der Neut and Wapenaar (2016) propose to remove the internal multiple reflections from the single-sided reflection response without model information. The performance of these schemes in 2D numerical data has been illustrated (Zhang and Staring, 2018), and the application to field data has not yet been realized. Wang et al. (2014, 2017) propose to eliminate artifacts due to reverse time migration of free-surface-related multiples in angle-domain common-image gathers or using the wavefield decomposition imaging condition. The success has been validated by numerical examples. Recently, revised Marchenko redatuming schemes have been introduced to remove the free-surface and internal multiple reflections in the image domain with the measured single-sided reflection response as input (Singh et al., 2015, 2017; Ravasi, 2017). Because Marchenko redatuming schemes create a virtual receiver inside the medium, they require an estimate of the first arrival of the focusing wavefield. Computing this estimate requires a macrovelocity model to be built before these methods can be applied. To our understanding, existing methods cannot eliminate the free-surface and internal multiple reflections together without any model information and adaptive filtering.

In this paper, we present a scheme to eliminate free-surface and internal multiple reflections from the acoustic single-sided reflec-

Manuscript received by the Editor 21 July 2018; revised manuscript received 27 August 2018; published online 3 December 2018.
[1]Corresponding author. Delft University of Technology, 2628 CN, Delft, The Netherlands. E-mail: l.zhang-1@tudelft.nl (corresponding author).
[2]Delft University of Technology, 2628 CN, Delft, The Netherlands. E-mail: e.c.slob@tudelft.nl.

tion response in one step. The paper is organized as follows: In the "Theory" section, we show how this scheme can be derived by starting with the revised Marchenko equations presented by Singh et al. (2017). Then, we show how a modification of the projection method of van der Neut and Wapenaar (2016) leads to the desired method. Finally, we show how in the new scheme free-surface and internal multiple reflections are eliminated and primary reflections are identified, captured, and stored in a new data set. In this processing only, the single-sided reflection response is required as input and the output contains only primary reflections. Thus, we argue that performing seismic migration on the new data set is more convenient than on the original data set to obtain a subsurface image. A numerical example section follows to show how well the scheme eliminates the free-surface and internal multiple reflections from the computed single-sided reflection response.

THEORY

We indicate the time as t and the position vector of a spatial location as $\mathbf{x} = (x, y, z)$, where z denotes the depth and (x, y) denote the horizontal coordinates. The pressure free surface $\partial\mathbf{D}_0$ is defined as $z_0 = 0$. For convenience, the coordinates at $\partial\mathbf{D}_0$ are denoted as $\mathbf{x}_0 = (\mathbf{x}_H, z_0)$, with $\mathbf{x}_H = (x, y)$. Similarly, the position vector of a point at an arbitrary depth level $\partial\mathbf{D}_i$ is denoted as $\mathbf{x}_i = (\mathbf{x}_H, z_i)$, where z_i denotes the depth level of $\partial\mathbf{D}_i$. The vertical axis points down, and we have $z_0 < z_i$. We express the acoustic impulse-reflection response as $R(\mathbf{x}'_0, \mathbf{x}_0, t)$, where $\mathbf{x}_0$ denotes the source position and $\mathbf{x}'_0$ denotes the receiver position, both located at the free surface $\partial\mathbf{D}_0$. The Green's function $G(\mathbf{x}_i, \mathbf{x}_0, t)$ is defined for an impulsive source that is excited at $\mathbf{x}_0$, and a receiver is positioned at the focal point $\mathbf{x}_i$. The Green's function is defined in the same physical medium as the measured single-sided reflection response. We define the truncated medium as $z_0 < z < z_i$ in the same way as Wapenaar et al. (2014). Inside the truncated medium, the properties of the medium are equal to the properties of the physical medium. Outside the truncated medium, the truncated medium is reflection-free. The focusing wavefield $f_1(\mathbf{x}_0, \mathbf{x}_i, t)$ is the solution of the homogeneous wave equation in the truncated medium and focuses at the focal point $\mathbf{x}_i$ at $t = 0$. The focusing and Green's functions can be partitioned into up- and downgoing constituents, and for this, we use pressure-normalized quantities.

We start with the 3D versions of the one-way reciprocity theorems for pressure-normalized wavefields and use them for depth levels z_0 and z_i. In the presence of a free surface at the acquisition level z_0, we have the Green's function representations (Singh et al., 2017)

$$G^-(\mathbf{x}_i, \mathbf{x}'_0, t) = \int_{\partial\mathbf{D}_0} d\mathbf{x}_0 \int_0^{+\infty} [R(\mathbf{x}'_0, \mathbf{x}_0, t') f_1^+(\mathbf{x}_0, \mathbf{x}_i, t - t') - rR(\mathbf{x}'_0, \mathbf{x}_0, t') f_1^-(\mathbf{x}_0, \mathbf{x}_i, t - t')] dt' - f_1^-(\mathbf{x}'_0, \mathbf{x}_i, t), \quad (1)$$

$$G^+(\mathbf{x}_i, \mathbf{x}'_0, -t) = -\int_{\partial\mathbf{D}_0} d\mathbf{x}_0 \int_{-\infty}^0 [R(\mathbf{x}'_0, \mathbf{x}_0, -t') f_1^-(\mathbf{x}_0, \mathbf{x}_i, t - t') - rR(\mathbf{x}'_0, \mathbf{x}_0, -t') f_1^+(\mathbf{x}_0, \mathbf{x}_i, t - t')] dt' + f_1^+(\mathbf{x}'_0, \mathbf{x}_i, t), \quad (2)$$

where superscripts $+$ and $-$ indicate the downgoing and upgoing fields, respectively. The reflection coefficient of the free surface is denoted as r. We write the downgoing focusing function and the Green's function as the sum of a direct part and a following coda:

$$f_1^+(\mathbf{x}_0, \mathbf{x}_i, t) = f_{1d}^+(\mathbf{x}_0, \mathbf{x}_i, t) + f_{1m}^+(\mathbf{x}_0, \mathbf{x}_i, t), \quad (3)$$

$$G^+(\mathbf{x}_i, \mathbf{x}_0, t) = G_d^+(\mathbf{x}_i, \mathbf{x}_0, t) + G_m^+(\mathbf{x}_i, \mathbf{x}_0, t), \quad (4)$$

where f_{1d}^+ and G_d^+ indicate the direct part, whereas f_{1m}^+ and G_m^+ indicate the following coda. The initial downgoing focusing function can be interpreted as the inverse of the initial downgoing Green's function, as Wapenaar et al. (2014) present

$$\int_{\partial\mathbf{D}_i} d\mathbf{x}_i \int_0^{+\infty} G_d^+(\mathbf{x}_i, \mathbf{x}''_0, t') f_{1d}^+(\mathbf{x}_0, \mathbf{x}_i, t - t') dt' = \delta(\mathbf{x}''_H - \mathbf{x}_H)\delta(t), \quad (5)$$

where $\delta(\mathbf{x}_H)$ is a spatially band-limited 2D delta function in space and $\delta(t)$ is a delta function in time. Equation 5 shows that G_d^+ is the inverse of f_{1d}^+ in the sense that it collapses f_{1d}^+ to a delta function in the horizontal coordinates and time. Following van der Neut and Wapenaar (2016), we apply this convolution integral operator to equations 1 and 2 to find

$$U^-(\mathbf{x}''_0, \mathbf{x}'_0, t) = \int_{\partial\mathbf{D}_0} d\mathbf{x}_0 \int_0^{+\infty} \{R(\mathbf{x}'_0, \mathbf{x}_0, t')[\delta(t - t')\delta(\mathbf{x}''_H - \mathbf{x}_H) + v_m^+(\mathbf{x}_0, \mathbf{x}''_0, t - t')] - rR(\mathbf{x}'_0, \mathbf{x}_0, t') v^-(\mathbf{x}_0, \mathbf{x}''_0, t - t')\} dt' - v^-(\mathbf{x}'_0, \mathbf{x}''_0, t), \quad (6)$$

$$U^+(\mathbf{x}''_0, \mathbf{x}'_0, -t) = -\int_{\partial\mathbf{D}_0} d\mathbf{x}_0 \int_{-\infty}^0 \{R(\mathbf{x}'_0, \mathbf{x}_0, -t') v^-(\mathbf{x}_0, \mathbf{x}''_0, t - t') - rR(\mathbf{x}'_0, \mathbf{x}_0, -t')[\delta(t - t')\delta(\mathbf{x}''_H - \mathbf{x}_H) + v_m^+(\mathbf{x}_0, \mathbf{x}''_0, t - t')]\} dt' + \delta(t)\delta(\mathbf{x}''_H - \mathbf{x}'_H) + v_m^+(\mathbf{x}'_0, \mathbf{x}''_0, t), \quad (7)$$

with $U^\mp$ defined as

$$U^\mp(\mathbf{x}''_0, \mathbf{x}'_0, \pm t) = \int_{\partial\mathbf{D}_i} d\mathbf{x}_i \int_0^{+\infty} G_d^+(\mathbf{x}_i, \mathbf{x}''_0, t') G^\mp(\mathbf{x}_i, \mathbf{x}'_0, \pm(t - t')) dt', \quad (8)$$

and v^- and v_m^+ are the convolved versions of f_1^- and f_{1m}^+ similar to what is shown in equation 8 for G^-. Because the convolved Green's and focusing functions in equations 6 and 7 are separated in time except for one time instant (van der Neut and Wapenaar, 2016), we limit the time window in which we evaluate equations 6 and 7 and end up with

$$v^-(\mathbf{x}'_0, \mathbf{x}''_0, t) = R(\mathbf{x}'_0, \mathbf{x}''_0, t) + \int_{\partial\mathbf{D}_0} d\mathbf{x}_0 \int_0^{+\infty} [R(\mathbf{x}'_0, \mathbf{x}_0, t') v_m^+(\mathbf{x}_0, \mathbf{x}''_0, t - t') - rR(\mathbf{x}'_0, \mathbf{x}_0, t') v^-(\mathbf{x}_0, \mathbf{x}''_0, t - t')] dt', \quad \text{for } 0 < t < t_2 \quad (9)$$

$$v_m^+(\mathbf{x}'_0,\mathbf{x}''_0,t) = -rR(\mathbf{x}'_0,\mathbf{x}''_0,-t) + \int_{\partial\mathbf{D}_0} d\mathbf{x}_0 \int_{-\infty}^{0} [R(\mathbf{x}'_0,\mathbf{x}_0,-t')v^-(\mathbf{x}_0,\mathbf{x}''_0,t-t') - rR(\mathbf{x}'_0,\mathbf{x}_0,-t')v_m^+(\mathbf{x}_0,\mathbf{x}''_0,t-t')]dt', \quad \text{for } 0 < t < t_2 \quad (10)$$

where t_2 denotes the minimum two-way traveltime from a surface point $\mathbf{x}'_0$ to the focusing level z_i and back to the surface point $\mathbf{x}''_0$. These two equations can be seen as the projected version of the revised Marchenko equations for the single-sided reflection response with free-surface related multiple reflections presented by Singh et al. (2017). These two equations can be solved for v^- and v_m^+ using only the single-sided reflection response (the f_{1d}^+ collapses to a delta function in the projected version). The obtained v^- and v_m^+ from equations 9 and 10 can be used to compute U^- from equation 6 as

$$U^-(\mathbf{x}''_0,\mathbf{x}'_0,t) = R(\mathbf{x}''_0,\mathbf{x}'_0,t) + \int_{\partial\mathbf{D}_0} d\mathbf{x}_0 \int_{0}^{+\infty} [R(\mathbf{x}'_0,\mathbf{x}_0,t')v_m^+(\mathbf{x}_0,\mathbf{x}''_0,t-t') - rR(\mathbf{x}'_0,\mathbf{x}_0,t')v^-(\mathbf{x}_0,\mathbf{x}''_0,t-t')]dt', \text{for} t_2 \le t < +\infty. \quad (11)$$

The explanation of U^- can be given as follows. When the focusing point is at, but just above, an actual reflector as shown in Figure 1a, the Green's function in equation 1 is the upgoing field at the surface generated by an impulsive source at the focusing point. The reflection from that reflector will be the first event in G^-. By convolving this Green's function with G_d^+ as given by equation 8, we have redatumed all focusing points at $\partial\mathbf{D}_i$ back to a location at the surface to obtain U^-. The first event in U^- indicated by the red arrow in Figure 1b has two-way traveltime t_2 and is the primary reflection of the reflector below our original focusing level. When the focusing point is far from a reflector, the value in U^- with two-way traveltime t_2 (indicated by the green arrow in Figure 1d) is zero and the first event in U^- (indicated by the red arrow in Figure 1d) has a longer two-way traveltime than t_2. We can now conclude that t_2 in equation 11 describes a fictitious focusing level in the subsurface, where we have focused to and projected back from. When the focusing level coincides with an actual subsurface reflector, the first event in U^- at time instant t_2 will be the primary reflection of that reflector with two-way traveltime t_2. Otherwise, the value in U^- at time instant t_2 will be zero. This means that U^- can be evaluated and its first event can be picked to represent a possible primary reflection event of the medium. The time instant t_2 can be chosen as τ, and we collect the value of U^- for each value of τ and store it in a new function containing only primary reflections. We can write it as

$$R_t(\mathbf{x}''_0,\mathbf{x}'_0,t=\tau) = U^-(\mathbf{x}''_0,\mathbf{x}'_0,\tau), \quad (12)$$

where R_t denotes the retrieved primary reflections.

Equation 12 shows that only primary reflections end up in R_t. Note that the free-surface and internal multiple reflections are removed in one step, where no model information and adaptive subtraction are required. The retrieved data set is more suitable for velocity model estimation and standard imaging than the original data.

EXAMPLE

The aim of the current method is to retrieve the primary reflections by removing the free-surface and internal multiple reflections in one step given the measured single-sided reflection response at the pressure free surface. A 2D numerical example is given to illustrate the method. Figure 2a and 2b shows the values for the acoustic velocity and density as functions of depth and horizontal position. The source emits a Ricker wavelet with a 20 Hz center frequency. Absorbing boundary conditions are applied at two sides and bottom of the model; the top boundary of the model is set as the free surface (the reflection coefficient of the free surface r is -1). We have computed the single-sided reflection responses with 601 sources and 601 receivers with spacing of 10 m at the free-surface boundary. One of the computed single-sided reflection responses $\widehat{R}(\mathbf{x}'_0,\mathbf{x}''_0,t)$ (the hat indicates that quantity has been convolved with the source wavelet) is shown in Figure 3a. Note that free-surface and internal multiple reflections occur and the later primary reflections labeled by P7, P8, and P9 cannot be identified. This reflection response is used as input to solve equations 9–11 for U^-. Then, the procedure as described using equation 12 leads to the retrieved data set $\widehat{R}_t(\mathbf{x}'_0,\mathbf{x}''_0,t)$ as shown in Figure 3b. Note that free-surface and internal multiple reflections visible in Figure 3a have disappeared, whereas the last three primary reflection events labeled by P7, P8, and P9, which cannot be distinguished from multiple reflections in Figure 3a, are clearly retrieved in Figure 3b.

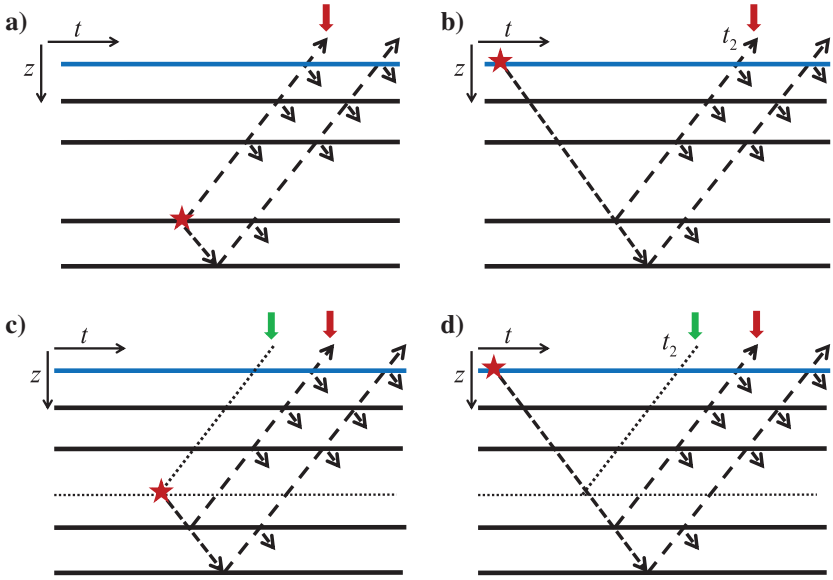

Figure 1. (a) The 1D sketch of the reciprocal of G^- in equation 1 with the focusing point at, but just above the third reflector, (b) the corresponding U^- in equation 8, (c) 1D sketch of the reciprocal of G^- in equation 1 with the focusing point far from the reflectors, and (d) the corresponding U^- in equation 8. The dotted horizontal line in (c and d) indicates the focusing level. In each plot, the red star indicates the focusing point (source), the red arrow indicates the first event, and the green arrow indicates a zero-valued event at t_2. The solid blue line indicates the pressure-free surface.

We pick the zero-offset traces from the data sets shown in Figure 3a and 3b and show them in Figure 4. It can be seen that free-surface and internal multiple reflections have been successfully removed, and primary reflections labeled P1, ..., P6 in Figure 3 have been well-retrieved. There is a mismatch of the last three primary reflections labeled by P7, P8, and P9 in Figure 3, which is illustrated in Figure 4. This is caused by the fact that the last three primary reflections are overlapped with multiple reflections in the trace from the original shot gather. The dotted red line (ER) indicates the trace from the retrieved data set, and both traces have been normalized by the same normalization factor.

Equations 9 and 10 can be solved by the Neumann series expansion or unconditionally convergent methods, e.g., the least-squares scheme or matrix inversion presented by Dukalski and de Vos (2018). In the derivation of the current method, we assumed a lossless medium. The method can be adapted to work with two-sided reflection and transmission data in dissipative media (Slob, 2016). We further assumed that the projected Green's functions and the focusing functions can be separated in time except for one time instant, that the source wavelet can be well-recovered and the evanescent waves are absent (Wapenaar et al., 2013) as well as refractions. These restrictions limit the application of the current method, but not more than existing methods that require model information or adaptive filtering before the free-surface and internal multiple reflections are removed. For situations in which these assumptions are fulfilled, the current method has a nearly perfect performance as is shown with the 2D numerical example.

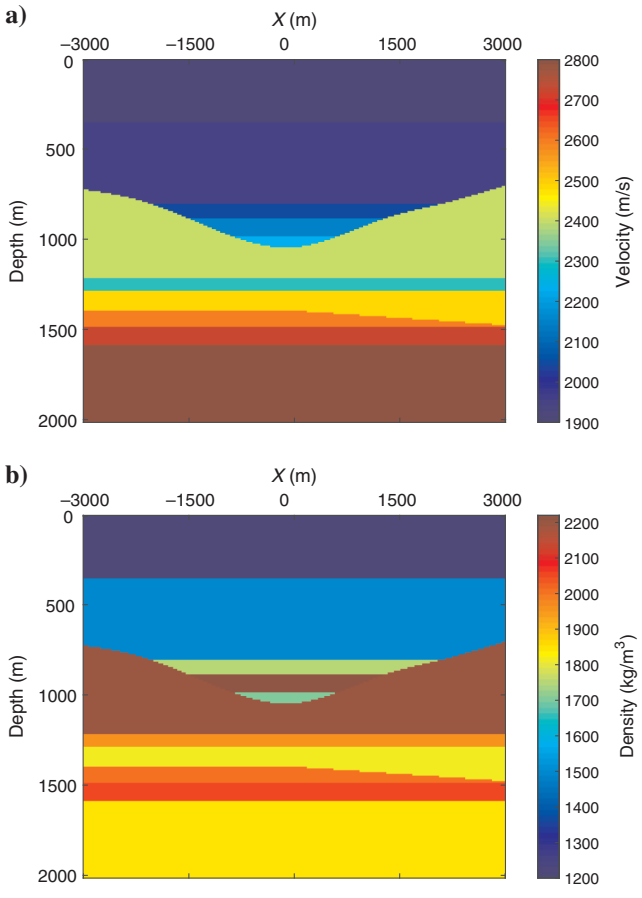

Figure 2. (a) The velocity and (b) density models that will be used to model the single-sided reflection response.

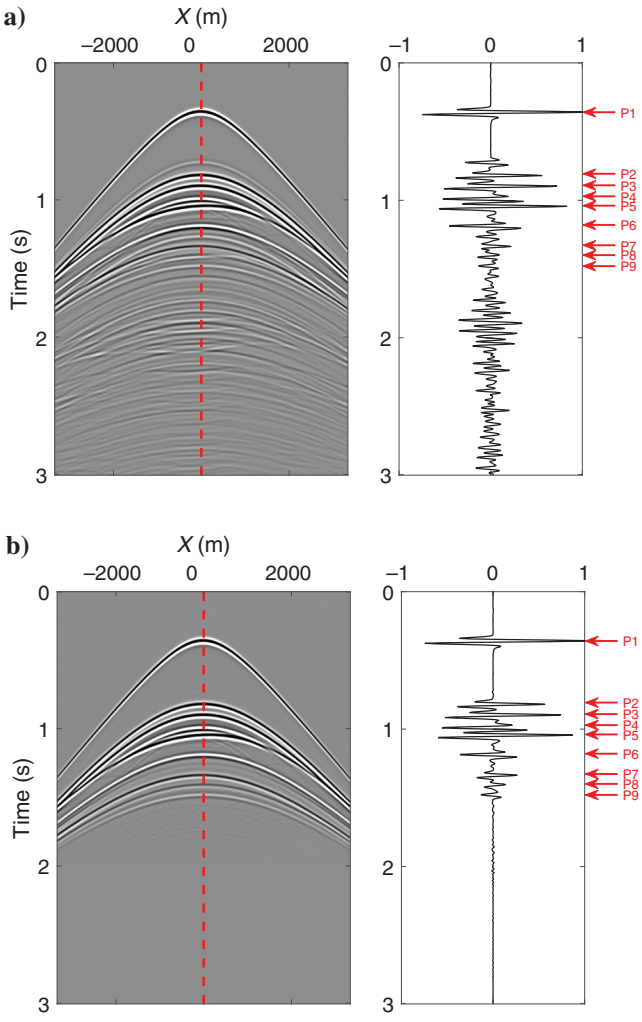

Figure 3. (a) The modeled reflection response and (b) the retrieved primary reflections. Dashed red lines indicate zero-offset traces plotted at the right side, P1, ..., P9 label the primary reflections.

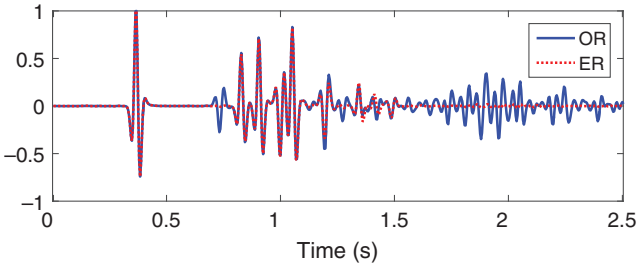

Figure 4. Comparison of zero-offset traces from Figure 3. The solid blue line (OR) comes from the original shot gather shown in Figure 3a, and the dotted red line (ER) comes from the retrieved primary reflections shown in Figure 3b.

CONCLUSION

We have shown that the single-sided reflection response can be used to remove its own free-surface and internal multiple reflections. The reflection response is convolved and correlated with an intermediate wavefield that exists within a specific time window. From this intermediate wavefield, the primary reflection is computed and stored in the new data set. The 2D numerical example shows that the method effectively removes free-surface and internal multiple reflections in one step without any model information. We expect that the current method can be used in seismic reflection imaging and monitoring of structures and processes in the earth's interior.

ACKNOWLEDGMENTS

This work is part of the Open Technology Program with project number 13939, which is financed by the NWO Domain Applied and Engineering Sciences. We would like to thank J. Blanch and two anonymous reviewers for their valuable suggestions. The 2D reflection response in this letter is generated with the finite-difference package in Thorbecke and Draganov (2011).

DATA AND MATERIALS AVAILABILITY

Data associated with this research are available and can be obtained by contacting the corresponding author.

REFERENCES

Dukalski, M., and K. de Vos, 2018, Marchenko inversion in a strong scattering regime including surface-related multiples: Geophysical Journal International, **212**, 760–776.

Löer, K., A. Curtis, and G. A. Meles, 2016, Relating source-receiver interferometry to an inverse-scattering series to derive a new method to estimate internal multiples: Geophysics, **81**, no. 3, Q27–Q40, doi: 10.1190/geo2015-0330.1.

Ravasi, M., 2017, Rayleigh-Marchenko redatuming for target-oriented, true-amplitude imaging: Geophysics, **82**, no. 6, S439–S452, doi: 10.1190/geo2017-0262.1.

Singh, S., R. Snieder, J. Behura, J. van der Neut, K. Wapenaar, and E. Slob, 2015, Marchenko imaging: Imaging with primaries, internal multiples, and free-surface multiples: Geophysics, **80**, no. 5, S165–S174, doi: 10.1190/geo2014-0494.1.

Singh, S., R. Snieder, J. van der Neut, J. Thorbecke, E. Slob, and K. Wapenaar, 2017, Accounting for free-surface multiples in Marchenko imaging: Geophysics, **82**, no. 1, R19–R30, doi: 10.1190/geo2015-0646.1.

Slob, E., 2016, Green's function retrieval and Marchenko imaging in a dissipative acoustic medium: Physical Review Letters, **116**, 164301, doi: 10.1103/PhysRevLett.116.164301.

Ten Kroode, P. E., 2002, Prediction of internal multiples: Wave Motion, **35**, 315–338, doi: 10.1016/S0165-2125(01)00109-3.

Thorbecke, J., and D. Draganov, 2011, Finite-difference modeling experiments for seismic interferometry: Geophysics, **76**, no. 6, H1–H18, doi: 10.1190/geo2010-0039.1.

van der Neut, J., and K. Wapenaar, 2016, Adaptive overburden elimination with the multidimensional Marchenko equation: Geophysics, **81**, no. 5, T265–T284, doi: 10.1190/geo2016-0024.1.

Verschuur, D., A. Berkhout, and K. Wapenaar, 1992, Adaptive surface-related multiple elimination: Geophysics, **57**, 1166–1177, doi: 10.1190/1.1443330.

Wang, Y., Y. Zheng, Q. Xue, X. Chang, T. W. Fei, and Y. Luo, 2017, Reverse time migration of multiples: Reducing migration artifacts using the wavefield decomposition imaging condition: Geophysics, **82**, no. 4, S307–S314, doi: 10.1190/geo2016-0354.1.

Wang, Y., Y. Zheng, L. Zhang, X. Chang, and Z. Yao, 2014, Reverse time migration of multiples: Eliminating migration artifacts in angle domain common image gathers: Geophysics, **79**, no. 6, S263–S270, doi: 10.1190/geo2013-0441.1.

Wapenaar, K., F. Broggini, E. Slob, and R. Snieder, 2013, Three-dimensional single-sided Marchenko inverse scattering, data-driven focusing, Green's function retrieval, and their mutual relations: Physical Review Letters, **110**, 084301, doi: 10.1103/PhysRevLett.110.084301.

Wapenaar, K., J. Thorbecke, J. van der Neut, F. Broggini, E. Slob, and R. Snieder, 2014, Marchenko imaging: Geophysics, **79**, no. 3, WA39–WA57, doi: 10.1190/geo2013-0302.1.

Weglein, A. B., 2016, Multiples: Signal or noise: Geophysics, **81**, no. 4, V283–V302, doi: 10.1190/geo2014-0486.1.

Weglein, A. B., F. A. Gasparotto, P. M. Carvalho, and R. H. Stolt, 1997, An inverse scattering series method for attenuating multiples in seismic reflection data: Geophysics, **62**, 1975–1989, doi: 10.1190/1.1444298.

Zhang, L., and M. Staring, 2018, Marchenko scheme based internal multiple reflection elimination in acoustic wavefield: Journal of Applied Geophysics, **159**, 429–433, doi: 10.1016/j.jappgeo.2018.09.024.